ACS OMEGA

http://pubs.acs.org/journal/acsodf

Article

Thermotropic Behavior and Structural Organization of C24:1 Sulfatide Dispersions and Its Mixtures with Cationic Bilayers

Lucas de Andrade, Evandro L. Duarte, M. Teresa Lamy, and Julio H. K. Rozenfeld*

Cite This: *ACS Omega* 2023, 8, 5306−5315

Read Online

ACCESS | Metrics & More | Article Recommendations | Supporting Information

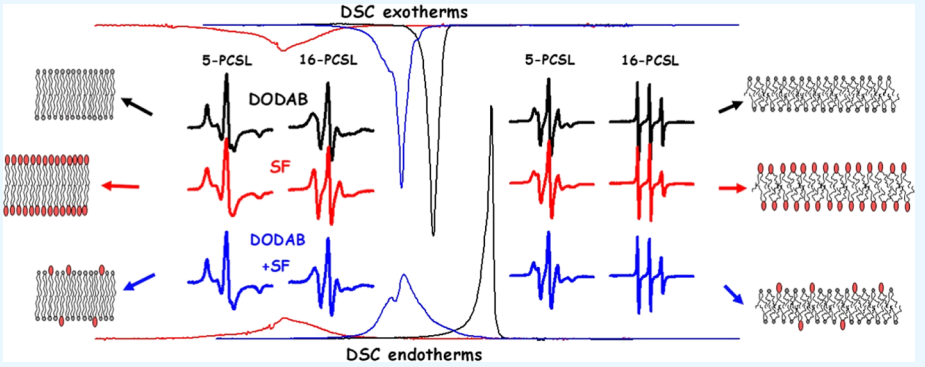

ABSTRACT: C24:1 sulfatide (SF) is an endogenous activator of type II NKT cells. The thermotropic behavior and structure of SF dispersions and its mixtures (4.8−16.6 mol %) with cationic dioctadecyldimethylammonium bromide (DODAB) bilayers were investigated by differential scanning calorimetry and electron paramagnetic resonance spectroscopy. The non-interdigitated lamellar structures formed by pure SF display broad thermal events around 27.5 °C when heated and cooled. These events disappear upon mixing with DODAB, showing complete lipid miscibility. SF decreases the DODAB gel-phase packing, with a consequent decrease in phase-transition temperatures and cooperativity upon heating. In contrast, SF increases the rigidity of the DODAB fluid phase, resulting in a smaller decrease in transition temperatures upon cooling. The hysteresis between heating and cooling decreased as the SF molar fraction increased. These effects on DODAB are similar to the ones described for other glycolipids, such as αGalCer and βGlcCer. This might be due to the orientation of the rigid and planar amide bond that connects their sphingoid bases and acyl chains, which result in a V-shaped conformation of the glycolipid molecules. The current results may be important to plan and develop new immunotherapeutic tools based on SF.

1. INTRODUCTION

Sulfatides (SFs) are galactosylceramides with an anionic sulfate group linked to the 3-*O* position of their sugar headgroup.[1] Their many isoforms are present in the kidneys, gastrointestinal tract, pancreatic islets of Langerhans, and, more abundantly, in the nervous system,[1,2] where they comprise 4−6% of myelin sheath lipids.[1,3] They are important to stabilize the myelin sheath,[4] not only by reinforcing contacts between apposed membranes[5] but also by forming domains that control protein traffic and organization.[6,7] Consequently, SF is associated with diseases such as multiple sclerosis,[8] Alzheimer's,[7] and metachromatic leukodystrophy.[9]

In addition to their structural functions, SFs also have immunoregulatory activity: it was recently shown that SFs with short-chain fatty acids are ligands of the innate immune receptor TLR4.[10] Moreover, SFs are endogenous ligands for type II NKT cells.[11] This is the case for the long and unsaturated C24:1 SF, which was shown to efficiently activate type II NKT cells.[12,13] Considering the possible therapeutic applications of type II NKT cells,[14,15] the development of carriers for SF is very important.

The cationic lipid dioctadecyldimethylammonium bromide (DODAB) has been employed to deliver nucleic acids[16] and hydrophobic drugs.[17] It has also been used as a safe and efficient antigen carrier,[18,19] which makes it an interesting candidate to deliver SF.

The structural characterization of delivery systems is essential to understand their function and efficiency.[20] Differential scanning calorimetry (DSC) provides important information on how temperature affects the organization of lipid dispersions and has been extensively employed to evaluate

Received: September 25, 2022
Accepted: January 20, 2023
Published: February 2, 2023

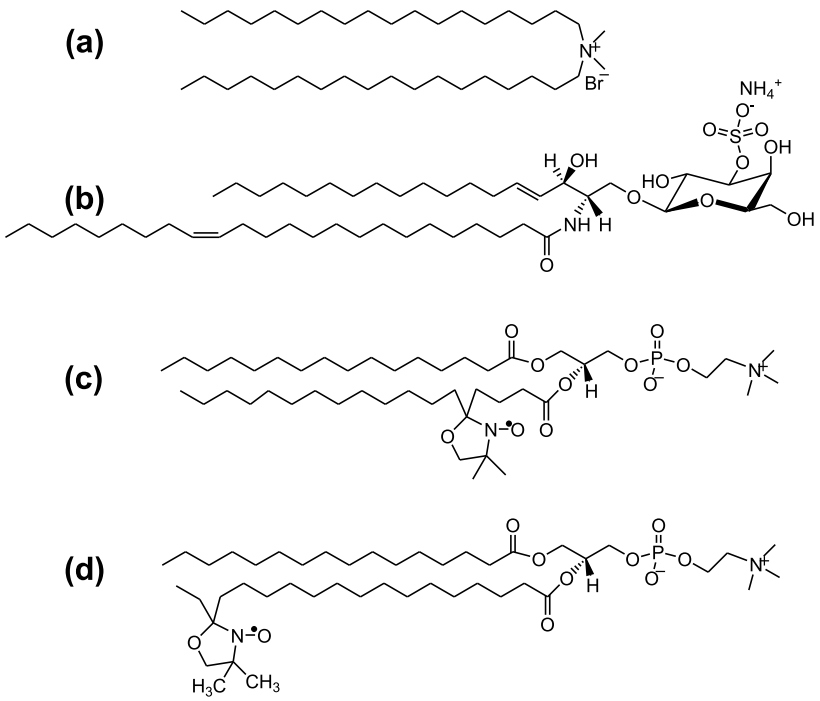

Figure 1. Chemical structures of DODAB (A), C24:1 SF (B), 5-PCSL (C), and 16-PCSL (D).

the energetics of phase transitions in lipid vesicles.[21] Continuous wave electron paramagnetic resonance (CW-EPR) spectroscopy is a powerful technique to investigate the structure of proteins[22] and lipid membranes.[23] In the latter case, CW-EPR is considered more sensitive than fluorescence spectroscopy to detect lipid-phase coexistence and interdigitation.[23,24]

In the present work, we use DSC and CW-EPR to characterize the thermotropic behavior and the structure of SF and DODAB + SF dispersions at different molar fractions.

2. EXPERIMENTAL METHODS

2.1. Materials. HEPES buffer, DODAB, (2*S*,3*S*,4*R*)-1-O-(a-D-galactosyl)-*N*-hexacosanoyl-2-amino-1,3,4-octadecanetriol (C24:1 SF), and spin label 1-palmitoyl-2-(*n*-doxylstearoyl)-*sn*-glycero-3-phosphocholine (*n*-PCSL, *n* = 5 or 16) were purchased from Sigma Chemical Co. (St. Louis, MO, USA). The chemical structures of lipids and spin labels are shown in Figure 1.

2.2. Preparation of Lipid Dispersions. Lipid dispersions were prepared as previously described.[25] Briefly, lipid films were prepared by drying chloroform/methanol 2:1 (v/v) solutions. The films were then hydrated in HEPES buffer (10 mM, pH 7.4) by vortexing and heating at 87 °C for 15 min to produce the vesicles. Dispersions were then allowed to reach room temperature prior to all experiments. For ESR experiments, 0.8 mol % 5-PCSL or 0.3 mol % 16-PCSL were added when preparing the lipid films. The final DODAB concentration was 2 mM. The final SF concentrations were 0.1, 0.2, or 0.4 mM, which correspond, respectively, to 4.8, 9, and 16.6 mol % of the total lipid concentration. A concentration of 2 mM SF was used in ESR experiments with pure glycolipid, in order to avoid spin−spin interactions.

2.3. Differential Scanning Calorimetry. Thermograms were obtained in a Microcal VP-DSC Microcalorimeter (Microcal Inc., Northampton, MA, USA). Heating and cooling rates were 20 °C/h, the feedback gain was high, and a 10 s filtering period was used. Scans were performed with at least two samples prepared in different days. A single annealing heating scan of 90 °C/h was performed prior to all experiments. The scans of all DODAB dispersions started at 20 °C in order to avoid the formation of a subgel phase, whose characteristic pre-transition peak at 36 °C could complicate the thermogram analyses.[26] The software MicroCal Origin was used to treat data and obtain thermodynamic parameters such as the phase-transition enthalpy (ΔH), the width at half-maximum ($T_{1/2}$), and the phase-transition temperature (T_m), which was considered the highest ΔC_p value.

2.4. EPR Spectroscopy. CW-EPR spectra at the X band (9.44 GHz) were obtained with a Bruker EMX spectrometer using a high-sensitivity ER4119HS cavity. The microwave power was 13.4 mW, the modulation frequency was 100 kHz, and the modulation amplitude was 1 G. The averaging number of scans was 20 for the temperature range of the gel phase and 5 for the temperature range of the fluid phase. A Bruker BVT-200 variable temperature device was used to control the sample temperatures. Experiments were performed at least twice, with samples prepared on different occasions. Empirical data correspond to the means of experiments with different samples, and standard deviations of these samples are shown as error bars.

The values of the maximum (A_{max}) and minimum (A_{min}) hyperfine splittings, as well as those of the low (h_{+1}), central (h_0), and high (h_{-1}) field line amplitudes were measured directly from spectra (see Figures 3 and 5).

The effective order parameter, S_{eff}, was calculated from the expression[27]

$$S_{eff} = \frac{A_{//} - A_{\perp}}{A_{ZZ} - (1/2)(A_{xx} + A_{yy})} \frac{a_o'}{a_o}$$

where $a_o' = (1/3)(A_{xx} + A_{yy} + A_{zz})$, $a_o = (1/3)(A_{//} + 2A_{\perp})$, $A_{//}$ (= A_{max}) is the maximum hyperfine splitting directly

https://doi.org/10.1021/acsomega.2c06189
ACS Omega 2023, 8, 5306−5315

measured in the spectrum, $A_{\perp} = A_{min} + 1.4\left[1 - \frac{A_{//} - A_{min}}{A_{zz} - (1/2)(A_{xx} + A_{yy})}\right]$, A_{min} is the measured inner hyperfine splitting (see Figure 5), and A_{xx}, A_{yy}, and A_{zz} are the principal values of the hyperfine tensor for doxylpropane.[28] Each experiment was performed at least two times. Error values account for standard deviations and are presented as error bars when larger than the symbols.

3. RESULTS

3.1. SF Decreases the Transition Temperature of DODAB Vesicles upon Heating and Cooling but Decreases the Transition Cooperativity Only upon Heating.

The heating and cooling thermograms of SF, DODAB, and DODAB + SF dispersions are shown in Figure 2.

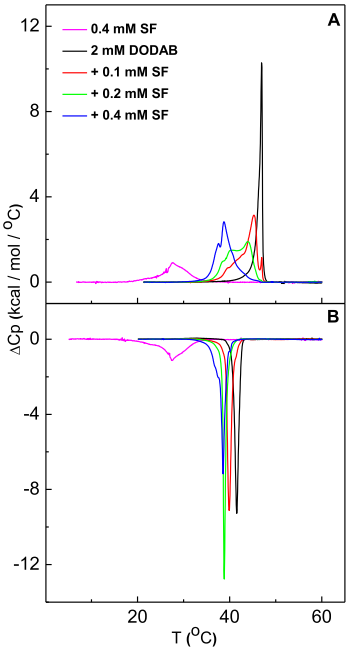

Figure 2. Typical heating (A) and cooling (B) thermograms of SF, DODAB, and DODAB + SF dispersions. The scan rate was 20 °C/h.

Pure SF dispersions display broad endothermic and exothermic events peaking around 27.5 °C; hence, no hysteresis upon heating and cooling is observed (Figure 2A,B). Although these thermogram profiles are significantly different from the ones previously described for C24:1 SF,[29] a direct comparison is difficult because the samples described earlier were more concentrated (15−22 mM), were prepared in a much higher ionic strength (2 M KCl), and were scanned at much higher rates (slower rates were 75 °C/h).[29] The scan rate of 20 °C/h used in the present work is the highest recommended for phospholipids[30] since it allows the measurement to be performed in thermodynamic equilibrium. Also, the microcalorimeter is more sensitive and allows for more diluted samples.

In contrast to SF, pure DODAB dispersions have a narrow endothermic transition around 47 °C when heated (Figure 2A) and a narrow exothermic peak around 41.5 °C when cooled (Figure 2B). The narrow peaks indicate that these phase transitions are cooperative, i.e., the conformational changes of one molecule are transmitted to the other molecules of the array, leading to a collective change of all molecules.[30,31] Similar thermograms, with narrow peaks and a hysteresis of 5.4 °C between heating and cooling, have been described for diluted DODAB dispersions in water.[32,33] These samples prepared in water have transition peaks upon heating and cooling around 44 and 39 °C, respectively.[32,33] A narrow peak around 47 °C has been described upon heating buffered samples,[25,34] suggesting that the increase in transition temperature results from the electrostatic shielding of the cationic DODAB headgroups.

In dispersions of DODAB + SF, the broad peaks around 27.5 °C disappear, suggesting a complete mixing of SF within the DODAB vesicles at all SF molar fractions tested (Figure 2A,B). Similar analyses of DSC thermograms have been previously used to access lipid miscibility.[35]

In the heating scans, the mixed DODAB + SF dispersions show broader peaks than pure DODAB, and these peaks are shifted to lower temperatures (Figure 2A), indicating that SF reduces the transition cooperativity and destabilize the gel phase of DODAB vesicles.

On the other hand, narrow peaks are observed for mixed DODAB + SF dispersions in the cooling scans (Figure 2B), indicating that the thermal transition is still rather cooperative when the samples are cooled. These narrow peaks are shifted to lower temperatures, and hysteresis is reduced as the SF molar fraction is increased. In fact, the hysteresis apparently disappears when 0.4 mM SF is mixed with 2 mM DODAB since the peaks upon heating and cooling occur at the same transition temperature (T_m), around 38.7 °C (Figures 2A,B). Tm and other thermodynamic parameters obtained from the thermograms are summarized in Table 1.

In Table 1, it is possible to observe that SF does not significantly alter the transition enthalpies (ΔH) of DODAB vesicles upon heating or cooling. SF also does not significantly change the transition cooperativity upon cooling as can be seen from the width at half-maximum of peaks ($T_{1/2}$), but it does decrease the transition cooperativity of DODAB upon heating since $T_{1/2}$ values increase with increasing SF concentration (Table 1 and Figure 2A).

Table 1. Thermodynamic Parameters of SF, DODAB, and DODAB + SF Dispersions

	heating			cooling		
dispersion	T_m[a](± s.d.)	ΔH(± s.d.)	$T_{1/2}$(± s.d.)	T_m[a](± s.d.)	ΔH(± s.d.)	$T_{1/2}$(± s.d.)
0.4 mM SF	27.6 ± 0.0	6.2 ± 0.7	4.9 ± 0.4	27.4 ± 0.0	−4.6 ± 3.0	4.2 ± 0.4
2 mM DODAB	46.9 ± 0.0	10.3 ± 0.2	0.6 ± 0.0	41.5 ± 0.0	−9.9 ± 0.2	0.8 ± 0.0
+0.1 mM SF	45.1 ± 0.1	11.8 ± 0.2	2.3 ± 0.0	39.7 ± 0.1	−11.8 ± 0.1	1.0 ± 0.1
+0.2 mM SF	43.6 ± 0.3	11.8 ± 0.0	6.7 ± 0.0	38.7 ± 0.0	−11 ± 0.1	0.4 ± 0.0
+0.4 mM SF	38.8 ± 0.0	10.9 ± 0.5	4.6 ± 1.6	38.6 ± 0.2	−10.4 ± 0.7	1.2 ± 0.6

[a]T_m was considered as the highest ΔC_p value.

https://doi.org/10.1021/acsomega.2c06189
ACS Omega 2023, 8, 5306−5315

3.2. DODAB Gel-Phase Packing Decreases in the Presence of SF. The structures of DODAB and DODAB + SF dispersions were compared by means of CW-EPR spectroscopy. This technique allows examining the microviscosity and packing of the membrane at different depths because it employs phospholipid probes labeled with a paramagnetic moiety at different positions.[23] For instance, the paramagnetic nitroxide group is located near the headgroup of 5-PCSL and at the end of the acyl chain in 16-PCSL (Figure 1). Hence, 5-PCSL gives information about the bilayer region closer to the aqueous interface and 16-PCSL gives information about the bilayer core. Figure 3 shows the spectra of 5-PCSL and 16-PCSL embedded in DODAB and DODAB + SF dispersions at temperatures below the gel−fluid transition.

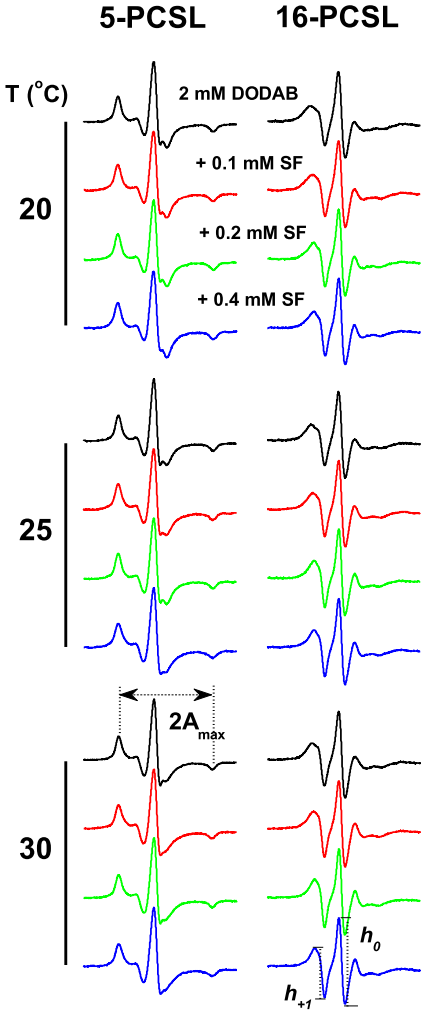

Figure 3. Effect of SF on the EPR spectra of 5-PCSL and 16-PCSL embedded in 2 mM DODAB bilayers at temperatures below the gel−fluid transition. The maximum hyperfine splitting (A_{max}) and the amplitudes of low (h_{+1}) and central (h_0) field lines are indicated. The total spectral width is 100 G.

In pure DODAB bilayers, the spectrum of 5-PCSL is more anisotropic than the spectrum of 16-PCSL (Figure 3), showing that these bilayers are more packed near the surface than in the core. This flexibility gradient toward the core is typical of DODAB bilayers in the gel phase[25,26] and is not changed by the presence of SF (Figure 3).

Since the spectrum profiles of both paramagnetic labels seem to be similar in pure DODAB and mixed DODAB + SF dispersions, empirical parameters obtained from the spectra can give more information about these structures (Figure 3). The maximum hyperfine splitting (A_{max}) is a useful parameter obtained from 5-PCSL spectra to evaluate the structure of bilayers in the gel phase (Figure 3) because it is sensitive to the viscosity and packing of the environment surrounding the label.[23] For instance, A_{max} values decrease as the viscosity or packing decreases.

The A_{max} values cannot be accurately measured in the spectra of 16-PCSL because they are more isotropic than the spectra of 5-PCSL (Figure 3). Hence, information about the structure of the bilayer core can be obtained from the ratio of the low and central field line amplitudes (h_{+1}/h_0) (Figure 3). The h_{+1}/h_0 values increase as the bilayers become less packed.[23]

Figure 4 shows the empirical parameters obtained from the spectra of 5-PCSL and 16-PCSL probing gel-phase dispersions.

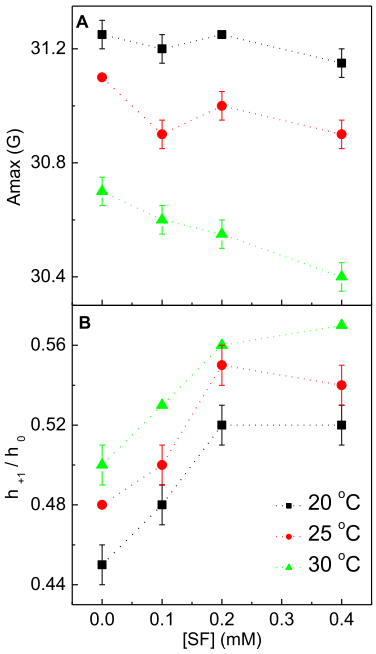

Figure 4. Effect of SF on the maximum hyperfine splitting (A_{max}) of 5-PCSL (A) and on the ratio of the low and the central field line amplitudes (h_{+1}/h_0) of 16-PCSL (B) embedded in 2 mM DODAB bilayers at the gel phase. Error bars indicate standard deviations of at least two experiments with different samples.

As expected, Figure 4A shows that the A_{max} values decrease as the temperature increases since membrane packing decreases as the temperature increases. A_{max} values also decrease as the SF fractions increase (Figure 4A), showing that SF decreases the superficial packing of DODAB bilayers.

Again as expected, Figure 4B shows that the h_{+1}/h_0 values increase when the temperature is increased and the membrane core packing is decreased. The h_{+1}/h_0 values also increase as the SF fraction increases (Figure 4B), suggesting that SF also decreases the packing at the DODAB bilayer core. The results in Figure 4A,B show that the DODAB gel-phase packing is decreased both at the surface and in the core in the presence of SF.

https://doi.org/10.1021/acsomega.2c06189
ACS Omega 2023, 8, 5306−5315

3.3. DODAB Fluid-Phase Packing Increases in the Presence of SF. Figure 5 shows the spectra of 5-PCSL and 16-PCSL embedded in DODAB and DODAB + SF dispersions at temperatures above the gel−fluid transition.

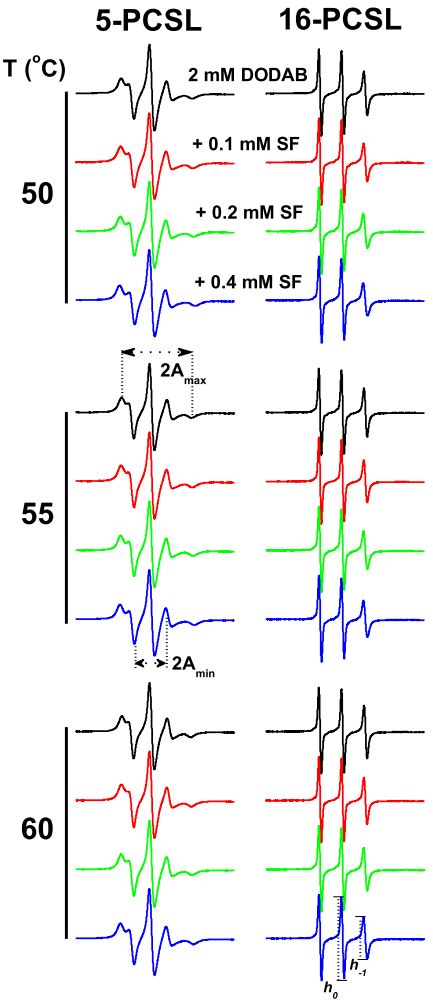

Figure 5. Effect of SF on the EPR spectra of 5-PCSL and 16-PCSL embedded in 2 mM DODAB bilayers at temperatures above the gel−fluid transition. The maximum hyperfine splitting (A_{max}) and the amplitudes of high (h_{-1}) and central (h_0) field lines are indicated. The total spectral width is 100 G.

The spectra of 5-PCSL shown in Figure 5 have thinner features than the ones observed at lower temperatures (Figure 3). The thinner features observed in Figure 5 indicate that the probes experience a fast movement on their long axis,[28] which is characteristic of a fluid yet organized structure near the membrane surface.

The spectra of 16-PCSL shown in Figure 5 have sharper peaks when compared to the ones at lower temperatures (Figure 3). The sharp peaks seen in Figure 5 indicate a fast and nearly isotropic movement of the nitroxide group at the bilayer core, which is typical of a spin label at the motional narrowing regime at the fluid phase of a membrane.[28]

The spectra of both 5-PCSL and 16-PCSL seem to be similar in the absence or presence of SF. Again, empirical parameters can be useful to compare the structures of DODAB and DODAB + SF dispersions (Figure 6).

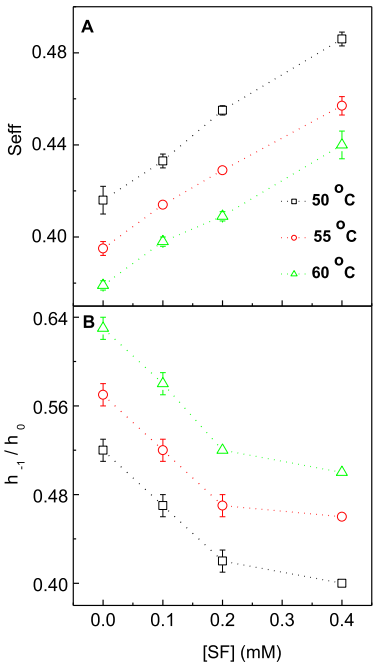

Figure 6. Effect of SF on the effective order parameter (S_{eff}) from 5-PCSL spectra (A) and on h_{-1}/h_0 ratios from 16-PCSL spectra (B) embedded in 2 mM DODAB bilayers at the fluid phase.

The values of the maximum and minimum hyperfine splittings (A_{max} and A_{min}) can be accurately measured from the anisotropic spectra of 5-PCSL in fluid-phase dispersions (Figure 5). These hyperfine splittings can then be used to calculate the effective order parameter (S_{eff}), as described in Section 2.4. S_{eff} is useful to evaluate the acyl chain order, although it is known to have contributions from the paramagnetic label mobility.[23,36] As expected, S_{eff} values decrease as the temperature increases (Figure 6A), indicating that the surface of the membrane becomes less ordered as the temperature increases. However, S_{eff} values increase with increasing SF fractions (Figure 6A), showing that SF increases the order near the surface of DODAB bilayers in the fluid phase.

The spectra of 16-PCSL are more isotropic and hinder the measurement of the hyperfine splittings, but the amplitudes of the high (h_{-1}) and central (h_0) field lines can be accurately measured (Figure 5). The ratio of these amplitudes (h_{-1}/h_0) can be used to evaluate the membrane viscosity or packing because the h_{-1}/h_0 ratio has an inverse relation with membrane viscosity: h_{-1}/h_0 values decrease as the membrane viscosity increases, for instance.[23,37]

As expected, it is possible to observe in Figure 6B that an increase in temperature results in an increase in the h_{-1}/h_0 ratio since the membrane viscosity decreases with temperature. In contrast, h_{-1}/h_0 values decrease with increasing SF fraction (Figure 6B), showing that SF increases the membrane core viscosity in the fluid phase. The results in Figure 6A,B show that the DODAB fluid-phase packing is increased both at the surface and in the core in the presence of SF.

3.4. Pure SF Forms Non-interdigitated Lamellar Structures. The EPR spectra of 5-PCSL and 16-PCSL in pure SF dispersions are shown in Figure 7. A concentration of 2 mM SF was used in order to avoid spin−spin interactions and to improve the signal-to-noise ratio.

https://doi.org/10.1021/acsomega.2c06189
ACS Omega 2023, 8, 5306−5315

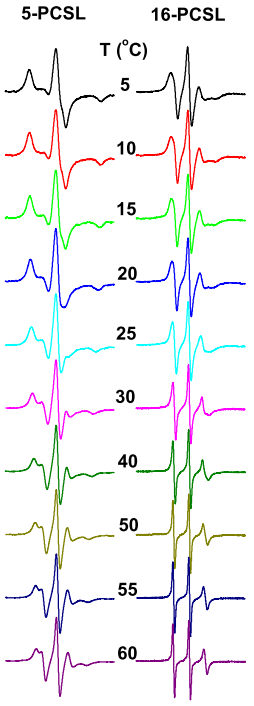

Figure 7. Effect of temperature on the ESR spectra of 5-PCSL and 16-PCSL embedded in dispersions of 2 mM SF. The total spectral width is 100 G.

The spectra of 5-PCSL are more anisotropic than the ones of 16-PCSL, suggesting the presence of a flexibility gradient at all temperatures tested (Figure 7). This gradient is very similar to the ones observed for DODAB and DODAB + SF (Figures 3 and 5) and indicates that SF self-assembles in non-interdigitated lamellar structures.[38]

As the temperature increases, the SF lamellae become more fluid, as the spectra of both probes become more isotropic (Figure 7). Indeed, a steep increase in fluidity can be observed between 25 and 30 °C, which is consistent with the broad thermal event around 27.5 °C observed in Figure 2. No coexistence of phases is observed in the 25−30 °C temperature range (Figure 7), which contrasts with the coexistence of rigid and fluid EPR signals around the gel−fluid transition of DODAB[39,40] (see the Supporting Information).

Figures 8 and 9 show the empirical parameters obtained from the EPR spectra of 5-PCSL and 16-PCSL at temperatures below and above the 25−30 °C range.

Figure 8 shows that the A_{max} values decrease and the h_{+1}/h_0 values increase when the temperature is increased, indicating a decrease in SF lamellar packing. The value of A_{max} at 20 °C is very similar to the one of pure DODAB at the same temperature (Figure 4A), but the value of h_{+1}/h_0 is much higher than the one of DODAB at this temperature (Figure 4B). This suggests that, while pure DODAB and pure SF have a similar packing near the surface, the SF lipid tails have more mobility than the ones of DODAB near the lamellar core at 20 °C.

Figure 9 shows that the S_{eff} values decrease and the h_{-1}/h_0 values increase when the temperature is increased, indicating a decrease in SF lamellar packing. The values of S_{eff} at the temperatures of 50, 55, and 60 °C are between 0.52 and 0.44, being much higher than the ones for pure DODAB (which range from 0.42 to 0.38) at the same temperatures (Figure 6A). Also, the values of h_{-1}/h_0 for SF (between 0.26 and 0.32) are much lower than the ones of pure DODAB (between 0.52 and 0.64) at the temperature range of 50−60 °C (Figure 4B). This suggests that the fluid lamellae of pure SF are more

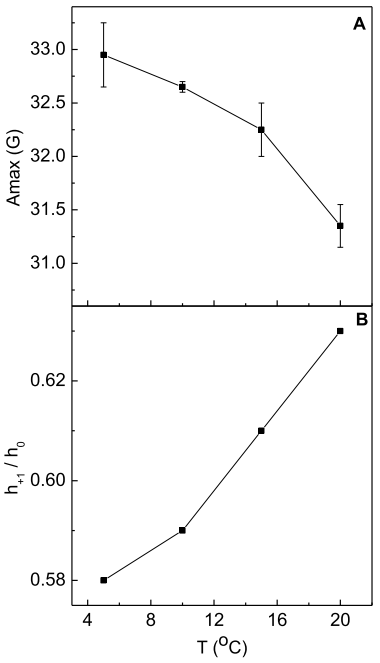

Figure 8. Values of the maximum hyperfine splitting (A_{max}) of 5-PCSL (A) and of the ratio of the low and the central field line amplitudes (h_{+1}/h_0) of 16-PCSL (B) embedded in 2 mM SF dispersions below the phase transition. Error bars indicate standard deviations of at least two experiments with different samples.

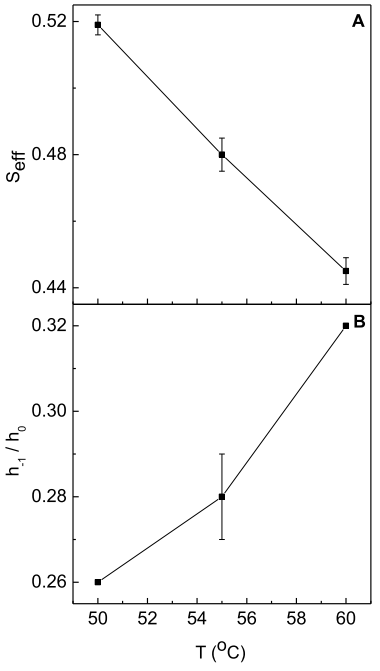

Figure 9. Values of the effective order parameter (S_{eff}) of 5-PCSL (A) and of ratios of the high and the central field line amplitudes (h_{-1}/h_0) of 16-PCSL (B) embedded in 2 mM SF dispersions above the phase transition. Error bars indicate standard deviations of at least two experiments with different samples.

https://doi.org/10.1021/acsomega.2c06189
ACS Omega 2023, 8, 5306−5315

ordered and packed both at the surface and the core than the bilayers of pure DODAB at this high-temperature range.

4. DISCUSSION

The single heating and cooling peaks at approximately 27.5 °C observed for pure C24:1 SF (Figure 2) contrast with the complex thermotropic behavior of C24:1 beta-glucosylceramide (βGlcCer), which presents several peaks upon heating and a single hysteretic peak upon cooling.[41] Considering that SF and βGlcCer have the same C24:1 ceramide moiety, the differences in thermotropic behavior could be attributed to the negative charge of the SF headgroup, whose electrostatic repulsion might hinder the formation of metastable phases and of high-temperature melting events observed for the neutral βGlcCer, which has a main phase-transition temperature around 66 °C when heated.[40,41] Electrostatic repulsion is an important factor in lipid-phase organization[42] and was shown to weaken intermolecular hydrogen bonding in SFs when compared to neutral cerebrosides.[29]

Despite their different thermotropic behaviors, pure SF and βGlcCer show similar structural organization in EPR spectroscopy assays: both form lamellar structures that are not interdigitated since a flexibility gradient is present at all temperatures (Figure 7).[40] Even though the C4-*trans* bond of the sphingosine base would facilitate the compact packing of the ceramide chains,[43,44] the 15-*cis* bond of the C24:1 acyl chain would increase the lateral space requirements (Figure 1), resulting in a decreased ceramide chain packing.[43,45] Accordingly, EPR experiments with 16-doxylstearate show that this *cis* double bond prevents any form of interdigitation in SFs.[46]

SF is miscible with DODAB at all fractions tested since the heating and cooling peaks at 27.5 °C disappear in the DODAB + SF dispersions (Figure 2). In agreement with that, SF does not significantly change the transition enthalpies (ΔH) of DODAB bilayers (Table1). On the other hand, SF has different effects on the phase-transition cooperativity of DODAB upon heating and cooling (Figure 2). Whereas ΔH is a measure of enthalpy change per molecule, cooperativity represents how the energy is distributed between the molecules in an array during a phase transition.[30]

SF decreases the transition temperature and cooperativity of DODAB bilayers upon heating but does not affect cooperativity upon cooling (Figure 2 and Table 1). The former effect could be attributed to the decrease in DODAB gel-phase packing induced by SF (Figures 3 and 4), while the latter could be attributed to the increase in DODAB fluid-phase rigidity by SF (Figures 5 and 6). Moreover, an increase in SF molar fraction induces a larger reduction of T_m values upon heating than upon cooling (Table 1). This might explain the decrease in hysteresis with the increase in SF molar fraction, as mentioned in Section 3.1 (Table 1).

Hysteresis is common in charged lipids such as DODAB.[32,33,47] It occurs when the transition paths upon heating and cooling are not the same, usually because domains of one phase are present within the matrix of another phase and the energy differences between the domains and the matrix result in strain tension.[47] It is possible that SF might be affecting the formation of these domains. For instance, it was shown that while the presence of two signals (representing two populations with different rigidities) are observed in the EPR spectra of 5-PCSL and 16-PCSL embedded in pure DODAB bilayers at 40 °C,[26,40] the presence of these two signals is already observed at 35 °C in mixtures with 0.4 mM βGlcCer.[40] Likewise, the Figure S1 (Supporting Information) shows that the two signals (two populations) are already visible at 35 °C in mixtures of DODAB with 0.2 and 0.4 mM SF. The negative charge of SF might enhance this effect when compared to the neutral βGlcCer, allowing the presence of two populations to be observed at the lower 0.2 mM SF fraction.

It is noteworthy that the decrease in phase-transition temperature and cooperativity, the decrease in the gel-phase packing, and the increase in fluid-phase rigidity of DODAB were observed not only in presence of the structurally similar SF and βGlcCer but also in the presence of alpha-galactosylceramide (αGalCer).[25] αGalCer is structurally very different from SF, not only because it lacks the sulfate group at the galactoside residue but also because this residue is α-linked to a ceramide that is made of a phytosphingosine base linked to a large saturated acyl chain.[25] However, SF and αGalCer share an important structural feature: an amide bond that connects the sphingoid base (sphingosine in SF, phytosphingosine in αGalCer) to the acyl chain (Figure 1).[25]

The amide bond has a planar and rigid trans configuration and adopts a perpendicular orientation toward the axes of the sphingoid and acyl chains.[48] In order to accommodate the polar headgroup into this rigid perpendicular orientation, the torsion angles spread out the sphingoid and acyl chains, resulting in a V-shaped molecular conformation.[48] This V-shaped conformation would result in a large lateral area requirement that would decrease the packing of the DODAB gel phase, as observed in Figure 4. The V-shaped conformation would also explain the increase in DODAB fluid-phase rigidity: the larger S_{eff} and smaller h_{-1}/h_0 values in Figure 6 indicate that the acyl chains of DODAB are more ordered and have less freedom of movement in the presence of SF, as they do in the presence of βGlcCer and αGalCer.[25,40] Paramagnetic-labeled galactosylceramides were also shown to increase the rigidity of membranes in the fluid phase.[49]

The SF ability to activate type II NKT cells[12] has been explored to modulate immune responses in autoimmune disease,[50] ischemic injury,[51] hepatitis,[52] sepsis,[53] and cancer.[15] SF has also been tested as an adjuvant for oral vaccine,[54] and as a component to improve drug delivery systems.[55] Despite its broad applications, no studies have so far focused on using carriers to improve the efficiency of delivery of SF to antigen presenting cells or to harness its immunological activity. This contrasts with the extensive research on carriers for αGalCer, which is a strong activator of type I NKT cells.[56]

DODAB could be a suitable carrier for SF, not only because it has been successfully employed as a vaccine adjuvant with other glycolipids[57] but also because it might facilitate the SF delivery to endosomes.[58] Endosomal delivery is very important for SF immune activity since its loading to CD1 presenting molecules occurs at this site.[59]

It was shown that less rigid liposomes tend to remain more time in the endosomes, and increase the efficiency of αGalCer presentation by antigen presenting cells.[60] Hence, the decrease in DODAB gel-phase packing by SF (Figures 3 and 4) might enhance its in vivo efficiency as well. Although that remains to be tested, the present work might contribute to the planning and development of efficient immunotherapeutic tools employing SF.

https://doi.org/10.1021/acsomega.2c06189
ACS Omega 2023, 8, 5306−5315

5. CONCLUSIONS

The thermotropic behavior and the structure of C24:1 SF dispersions and its mixtures with cationic DODAB bilayers were investigated through DSC and EPR spectroscopy. Non-interdigitated lamellar structures were formed when SF films were hydrated above 80 °C. These lamellar structures displayed broad thermal events peaking around 27.5 °C when heated and cooled. These peaks disappeared when SF was mixed with DODAB, suggesting a complete miscibility of up to 16 mol % SF in DODAB bilayers.

SF decreased the DODAB gel-phase packing, resulting in a decrease in transition temperatures and cooperativity upon heating. On the other hand, SF did not significantly affect the cooperativity and produced a smaller decrease in transition temperatures upon cooling because it increased the DODAB fluid-phase rigidity. The hysteresis between the heating and cooling of DODAB bilayers decreased as the SF molar fraction was increased.

The effects of SF on the molecular organization of DODAB bilayers are similar to the ones described for other glycolipids, such as αGalCer and βGlcCer. This might be due to the orientation of the rigid and planar amide bond that connects their sphingoid bases and acyl chains, which result in a V-shaped conformation of the glycolipid molecules. The results shown here may be important to plan and develop new immunotherapeutic tools based on SF.

■ ASSOCIATED CONTENT

Supporting Information

The Supporting Information is available free of charge at https://pubs.acs.org/doi/10.1021/acsomega.2c06189.

EPR spectra of 5-PCSL and 16-PCSL embedded in 2 mM DODAB or 2 mM DODAB + SF bilayers around the gel−fluid transition; arrows indicate the features of a more isotropic component which coexists with the typical gel phase signal; DSC thermograms of 2 mM DODAB (experimental parameters detailed in the study); DSC thermograms of 0.4 mM SF (experimental parameters detailed in the study); DSC thermograms of 2 mM DODAB + 0.1 mM SF (experimental parameters detailed in the study); DSC thermograms of 2 mM DODAB + 0.2 mM SF (experimental parameters detailed in the study); DSC thermograms of 2 mM DODAB + 0.4 mM SF (experimental parameters detailed in the study); individual EPR spectra—5-PCSL (experimental parameters detailed in the study); and individual EPR spectra−16-PCSL (experimental parameters detailed in the study) (PDF)

■ AUTHOR INFORMATION

Corresponding Author

Julio H. K. Rozenfeld − *Departamento de Biofísica, Escola Paulista de Medicina, Universidade Federal de São Paulo, 04023-062 São Paulo, São Paulo, Brazil;* orcid.org/0000-0002-5458-5329; Phone: +55 11 5576 4848 ext. 2340; Email: julio.rozenfeld@unifesp.br

Authors

Lucas de Andrade − *Departamento de Biofísica, Escola Paulista de Medicina, Universidade Federal de São Paulo, 04023-062 São Paulo, São Paulo, Brazil;* orcid.org/0000-0002-2355-5266

Evandro L. Duarte − *Instituto de Física, Universidade de São Paulo, 05508090 São Paulo, São Paulo, Brazil;* orcid.org/0000-0001-5550-6541

M. Teresa Lamy − *Instituto de Física, Universidade de São Paulo, 05508090 São Paulo, São Paulo, Brazil;* orcid.org/0000-0001-6616-6546

Complete contact information is available at: https://pubs.acs.org/10.1021/acsomega.2c06189

Notes

The authors declare no competing financial interest.

■ ACKNOWLEDGMENTS

This work was supported by grants #2016/19077-1, #2016/13368-4, and #2021/01593-1, São Paulo Research Foundation (FAPESP). This study was financed in part by the Coordenação de Aperfeiçoamento de Pessoal de Nível Superior—Brasil (CAPES)—Finance Code 001. L.d.A. was supported by grant #2020/01417-6, São Paulo Research Foundation (FAPESP) and M.T.L. is the recipient of a CNPq research fellowship. From Brazil, the National Council for Scientific and Technological Development (CNPq − 465259/2014-6), the Coordination for the Improvement of Higher Education Personnel (CAPES), the National Institute of Science and Technology Complex Fluids (INCT-FCx), and the São Paulo Research Foundation (FAPESP − 2014/50983-3).

■ REFERENCES

(1) Blomqvist, M.; Zetterberg, H.; Blennow, K.; Månsson, J. E. Sulfatide in health and disease. The evaluation of sulfatide in cerebrospinal fluid as a possible biomarker for neurodegeneration. *Mol. Cell. Neurosci.* **2021**, *116*, 103670.

(2) Takahashi, T.; Suzuki, T. Role of sulfatide in normal and pathological cells and tissues. *J. Lipid Res.* **2012**, *53*, 1437−1450.

(3) Eckhardt, M. The role and metabolism of sulfatide in the nervous system. *Mol. Neurobiol.* **2008**, *37*, 93−103.

(4) Schmitt, S.; Cantuti Castelvetri, L. C.; Simons, M. Metabolism and functions of lipids in myelin. *Biochim. Biophys. Acta, Mol. Cell Biol. Lipids* **2015**, *1851*, 999−1005.

(5) Boggs, J. M.; Gao, W.; Hirahara, Y. Myelin glycosphingolipids, galactosylceramide and sulfatide, participate in carbohydrate-carbohydrate interactions between apposed membranes and may form glycosynapses between oligodendrocyte and/or myelin membranes. *Biochim. Biophys. Acta, Gen. Subj.* **20081780**, *1780*, 445−455.

(6) Baron, W.; Hoekstra, D. On the biogenesis of myelin membranes: sorting, trafficking and cell polarity. *FEBS Lett.* **2010**, *584*, 1760−1770.

(7) Grassi, S.; Prioni, S.; Cabitta, L.; Aureli, M.; Sonnino, S.; Prinetti, A. The role of 3-O-Sulfogalactosylceramide, sulfatide, in the lateral organization of myelin membrane. *Neurochem. Res.* **2016**, *41*, 130−143.

(8) Yahara, S.; Kawamura, N.; Kishimoto, Y.; Saida, T.; Tourtellotte, W. W. A change in the cerebrosides and sulfatides in a demyelinating nervous system: development of the methodology and study of multiple sclerosis and Wallerian degeneration. *J. Neurol. Sci.* **1982**, *54*, 303−315.

(9) Batzios, S. P.; Zafeiriou, D. I. Developing treatment options for metachromatic leukodystrophy. *Mol. Genet. Metab.* **2012**, *105*, 56−63.

(10) Su, L.; Athamna, M.; Wang, Y.; Wang, J.; Freudenberg, M.; Yue, T.; Wang, J.; Moresco, E. M. Y.; He, H.; Zor, T.; Beutler, B. Sulfatides are endogenous ligands for the TLR4-MD-2 complex. *Proc. Natl. Acad. Sci. U.S.A.* **2021**, *118*, No. e2105316118.

(11) Singh, A. K.; Tripathi, P.; Cardell, S. L. Type II NKT cells: an elusive population with immunoregulatory properties. *Front. Immunol.* **2018**, *9*, 1969.

(12) Blomqvist, M.; Rhost, S.; Teneberg, S.; Löfbom, L.; Østerbye, T.; Brigl, M.; Månsson, J. E.; Cardell, S. L. Multiple tissue-specific isoforms of sulfatide activate CD1d-restricted type II NKT cells. *Eur. J. Immunol.* **2009**, *39*, 1726−1735.
(13) Rhost, S.; Löfbom, L.; Rynmark, B. M.; Pei, B.; Månsson, J. E.; Teneberg, S.; Blomqvist, M.; Cardell, S. L. Identification of novel glycolipid ligands activating a sulfatide-reactive, CD1d-restricted, type II natural killer T lymphocyte. *Eur. J. Immunol.* **2012**, *42*, 2851−2860.
(14) Dhodapkar, M. V.; Kumar, V. Type II NKT cells and their emerging role in health and disease. *J. Immunol.* **2017**, *198*, 1015−1021.
(15) Kato, S.; Berzofsky, J. A.; Terabe, M. Possible therapeutic application of targeting type II natural killer T cell-mediated suppression of tumor immunity. *Front. Immunol.* **2018**, *9*, 314.
(16) Silva, J. N.; Oliveira, A. C. N.; Casal, M. P. P. A.; Gomes, A. C.; Coutinho, P. J.; Coutinho, O. P.; Oliveira, M. R. DODAB: monoolein-based lipoplexes as non-viral vectors for transfection of mammalian cells. *Biochim. Biophys. Acta, Biomembr.* **2011**, *1808*, 2440−2449.
(17) Oliveira, T. R.; Benatti, C. R.; Lamy, M. T. Structural characterization of the interaction of the polyene antibiotic Amphotericin B with DODAB bicelles and vesicles. *Biochim. Biophys. Acta, Biomembr.* **2011**, *1808*, 2629−2637.
(18) Rozenfeld, J. H. K.; Silva, S. R.; Ranéia, P. A.; Faquim-Mauro, E.; Carmona-Ribeiro, A. M. Stable assemblies of cationic bilayer fragments and CpG oligonucleotide with enhanced immunoadjuvant activity in vivo. *J. Controlled Release* **2012**, *160*, 367−373.
(19) Pedersen, G. K.; Andersen, P.; Christensen, D. Immunocorrelates of CAF family adjuvants. *Semin. Immunol.* **2018**, *39*, 4−13.
(20) Watson, D. S.; Endsley, A. N.; Huang, L. Design considerations for liposomal vaccines: influence of formulation parameters on antibody and cell-mediated immune responses to liposome associated antigens. *Vaccine* **2012**, *30*, 2256−2272.
(21) Biltonen, R. L.; Lichtenberg, D. The use of differential scanning calorimetry as a tool to characterize liposome preparations. *Chem. Phys. Lipids* **1993**, *64*, 129−142.
(22) Reichenwallner, J.; Oehmichen, M. T.; Schmelzer, C. E.; Hauenschild, T.; Kerth, A.; Hinderberger, D. Exploring the pH-induced functional phase space of human serum albumin by EPR spectroscopy. *Magnetochemistry* **2018**, *4*, 47.
(23) Rozenfeld, J. H. K.; Duarte, E. L.; Oliveira, T. R.; Lamy, M. T. Structural insights on biologically relevant cationic membranes by ESR spectroscopy. *Biophys. Rev.* **2017**, *9*, 633−647.
(24) Boggs, J. M.; Rangaraj, G.; Watts, A. Behavior of spin labels in a variety of interdigitated lipid bilayers. *Biochim. Biophys. Acta, Biomembr.* **1989**, *981*, 243−253.
(25) Martins, L. S.; Duarte, E. L.; Lamy, M. T.; Rozenfeld, J. H. K. Supramolecular organization of α-galactosylceramide in pure dispersions and in cationic DODAB bilayers. *Chem. Phys. Lipids* **2020**, *232*, 104963.
(26) Rozenfeld, J. H.; Duarte, E. L.; Barbosa, L. R.; Lamy, M. T. The effect of an oligonucleotide on the structure of cationic DODAB vesicles. *Phys. Chem. Chem. Phys.* **2015**, *17*, 7498−7506.
(27) Boggs, J. M.; Rangaraj, G. Phase transitions and fatty acid spin label behavior in interdigitated lipid phases induced by glycerol and polymyxin. *Biochim. Biophys. Acta, Biomembr.* **1985**, *816*, 221−233.
(28) Hubbell, W. L.; McConnell, H. M. Molecular motion in spin-labeled phospholipids and membranes. *J. Am. Chem. Soc.* **1971**, *93*, 314.
(29) Boggs, J. M.; Koshy, K. M.; Rangaraj, G. Influence of structural modifications on the phase behavior of semi-synthetic cerebroside sulfate. *Biochim. Biophys. Acta, Biomembr.* **1988**, *938*, 361−372.
(30) Mason, J. T. Investigation of phase transitions in bilayer membranes. *Methods Enzymol.* **1998**, *295*, 468−494.
(31) Vignoli Muniz, G. S.; Duarte, E. L.; Lorenzón, E. N.; Cilli, E. M.; Lamy, M. T. What different physical techniques can disclose about disruptions on membrane structure caused by the antimicrobial peptide Hylin a1 and a more positively charged analogue. *Chem. Phys. Lipids* **2022**, *243*, 105173.
(32) Cocquyt, J.; Olsson, U.; Olofsson, G.; Van der Meeren, P. Thermal transitions of DODAB vesicular dispersions. *Colloid Polym. Sci.* **2005**, *283*, 1376−1381.
(33) Wu, F. G.; Yu, Z. W.; Ji, G. Formation and transformation of the subgel phase in dioctadecyldimethylammonium bromide aqueous dispersions. *Langmuir* **2011**, *27*, 2349−2356.
(34) Linseisen, F. M.; Bayerl, S.; Bayerl, T. M. 2H-NMR and DSC study of DPPC-DODAB mixtures. *Chem. Phys. Lipids* **1996**, *83*, 9−23.
(35) Nakano, M.; Inoue, R.; Koda, M.; Baba, T.; Matsunaga, H.; Natori, T.; Handa, T. Anomeric effects on the stability of bilayers of galactosylphytoceramides and on the interaction with phospholipids. *Langmuir* **2000**, *16*, 7156−7161.
(36) Schindler, H.; Seelig, J. EPR spectra of spin labels in lipid bilayers. *J. Chem. Phys.* **1973**, *59*, 1841−1850.
(37) Marsh, D. In *Spin Labeling: Theory and Applications*; Berliner, L. J., Reuben, J., Eds.; Plenum Press: New York, 1989; Vol. *8*, pp 255−303.
(38) Rozenfeld, J. H. K.; Duarte, E. L.; Ruysschaert, J. M.; Lonez, C.; Lamy, M. T. Structural characterization of novel cationic diC16-amidine bilayers: Evidence for partial interdigitation. *Biochim. Biophys. Acta, Biomembr.* **2015**, *1848*, 127−133.
(39) Benatti, C. R.; Feitosa, E.; Fernandez, R. M.; Lamy-Freund, M. T. Structural and thermal characterization of dioctadecyldimethylammonium bromide dispersions by spin labels. *Chem. Phys. Lipids* **2001**, *111*, 93−104.
(40) Martins, L. S.; Nomura, D. A.; Duarte, E. L.; Riske, K. A.; Lamy, M. T.; Rozenfeld, J. H. Structural characterization of cationic DODAB bilayers containing C24: 1 β-glucosylceramide. *Biochim. Biophys. Acta, Biomembr.* **2019**, *1861*, 643−650.
(41) Björkqvist, Y. J. E.; Brewer, J.; Bagatolli, L. A.; Slotte, J. P.; Westerlund, B. Thermotropic behavior and lateral distribution of very long chain sphingolipids. *Biochim. Biophys. Acta, Biomembr.* **2009**, *1788*, 1310−1320.
(42) Epand, R. M.; Hui, S. W. Effect of electrostatic repulsion on the morphology and thermotropic transitions of anionic phospholipids. *FEBS Lett.* **1986**, *209*, 257−260.
(43) Löfgren, H.; Pascher, I. Molecular arrangements of sphingolipids. The monolayer behaviour of ceramides. *Chem. Phys. Lipids* **1977**, *20*, 273−284.
(44) Brockman, H. L.; Momsen, M. M.; Brown, R. E.; He, L.; Chun, J.; Byun, H. S.; Bittman, R. The 4, 5-double bond of ceramide regulates its dipole potential, elastic properties, and packing behavior. *Biophys. J.* **2004**, *87*, 1722−1731.
(45) Maula, T.; Al Sazzad, M. A.; Slotte, J. P. Influence of hydroxylation, chain length, and chain unsaturation on bilayer properties of ceramides. *Biophys. J.* **2015**, *109*, 1639−1651.
(46) Boggs, J. M.; Koshy, K. M.; Rangaraj, G. Interdigitated lipid bilayers of long acyl chain species of cerebroside sulfate. A fatty acid spin label study. Biochimica et. *Biochim. Biophys. Acta, Biomembr.* **1988**, *938*, 373−385.
(47) Lee, A. G. Lipid phase transitions and phase diagrams I. Lipid phase transitions. *Biochim. Biophys. Acta, Rev. Biomembr.* **1977**, *472*, 237−281.
(48) Pascher, I. Molecular arrangements in sphingolipids Conformation and hydrogen bonding of ceramide and their implication on membrane stability and permeability. *Biochim. Biophys. Acta, Biomembr.* **1976**, *455*, 433−451.
(49) Sharom, F. J.; Grant, C. W. Glycosphingolipids in membrane architecture. *J. Supramol. Struct.* **1977**, *6*, 249−258.
(50) Jahng, A.; Maricic, I.; Aguilera, C.; Cardell, S.; Halder, R. C.; Kumar, V. Prevention of autoimmunity by targeting a distinct, noninvariant CD1d-reactive T cell population reactive to sulfatide. *J. Exp. Med.* **2004**, *199*, 947−957.
(51) Yang, S. H.; Lee, J. P.; Jang, H. R.; Cha, R. H.; Han, S. S.; Jeon, U. S.; Kim, D. K.; Song, J.; Lee, D. S.; Kim, Y. S. Sulfatide-reactive natural killer T cells abrogate ischemia-reperfusion injury. *J. Am. Soc. Nephrol.* **2011**, *22*, 1305−1314.

https://doi.org/10.1021/acsomega.2c06189
ACS Omega 2023, 8, 5306−5315

(52) Halder, R. C.; Aguilera, C.; Maricic, I.; Kumar, V. Type II NKT cell−mediated anergy induction in type I NKT cells prevents inflammatory liver disease. *J. Clin. Invest.* **2007**, *117*, 2302−2312.
(53) Kwiecinski, J.; Rhost, S.; Löfbom, L.; Blomqvist, M.; Månsson, J. E.; Cardell, S. L.; Jin, T. Sulfatide attenuates experimental Staphylococcus aureus sepsis through a CD1d-dependent pathway. *Infect. Immun.* **2013**, *81*, 1114−20.
(54) Albutti, A.; Longet, S.; McEntee, C. P.; Quinn, S.; Liddicoat, A.; Rîmniceanu, C.; Lycke, N.; Lynch, L.; Cardell, S.; Lavelle, E. C. Type II NKT cell agonist, sulfatide, is an effective adjuvant for oral heat-killed cholera vaccines. *Vaccines* **2021**, *9*, 619.
(55) Shao, K.; Hou, Q.; Duan, W.; Go, M. L.; Wong, K. P.; Li, Q. T. Intracellular drug delivery by sulfatide-mediated liposomes to gliomas. *J. Controlled Release* **2006**, *115*, 150−157.
(56) Macho-Fernandez, E.; Cruz, L. J.; Ghinnagow, R.; Fontaine, J.; Bialecki, E.; Frisch, B.; Trottein, F.; Faveeuw, C. Targeted delivery of α-galactosylceramide to CD8α+ dendritic cells optimizes type I NKT cell−based antitumor responses. *J. Immunol.* **2014**, *193*, 961−969.
(57) Davidsen, J.; Rosenkrands, I.; Christensen, D.; Vangala, A.; Kirby, D.; Perrie, Y.; Agger, E. M.; Andersen, P. Characterization of cationic liposomes based on dimethyldioctadecylammonium and synthetic cord factor from M. tuberculosis (trehalose 6, 6′-dibehenate)—a novel adjuvant inducing both strong CMI and antibody responses. *Biochim. Biophys. Acta, Biomembr.* **2005**, *1718*, 22−31.
(58) Korsholm, K. S.; Agger, E. M.; Foged, C.; Christensen, D.; Dietrich, J.; Andersen, C. S.; Geisler, C.; Andersen, P. The adjuvant mechanism of cationic dimethyldioctadecylammonium liposomes. *Immunology* **2007**, *121*, 216−26.
(59) Roy, K. C.; Maricic, I.; Khurana, A.; Smith, T. R.; Halder, R. C.; Kumar, V. Involvement of secretory and endosomal compartments in presentation of an exogenous self-glycolipid to type II NKT cells. *J. Immunol.* **2008**, *180*, 2942−2950.
(60) Nakamura, T.; Kuroi, M.; Harashima, H. Influence of endosomal escape and degradation of α-galactosylceramide loaded liposomes on CD1d antigen presentation. *Mol. Pharm.* **2015**, *12*, 2791−2799.

https://doi.org/10.1021/acsomega.2c06189
ACS Omega 2023, 8, 5306−5315